RSC Advances

PAPER

View Article Online
View Journal | View Issue

Cite this: *RSC Adv.*, 2021, **11**, 6655

Highly flexible and free-standing carbon nanotube/hollow carbon nanocage hybrid films for high-performance supercapacitors†

Qiang Qiang Shi, Hang Zhan, Yu Zhang and Jian Nong Wang *

Received 16th November 2020
Accepted 18th January 2021

DOI: 10.1039/d0ra09710a

rsc.li/rsc-advances

Carbon nanotubes (CNTs) have been considered as promising electrode materials for energy storage devices, especially flexible electronics owing to their excellent electrical, physicochemical and mechanical properties. However, the severe aggregation between CNTs significantly reduces the electrochemically active surface areas and thus degrades the electrochemical properties. In this study, we demonstrate a facile layer-by-layer strategy toward preparing a CNT/hollow carbon nanocage (HCNC) hybrid film. Through electrochemically removing the impurities in CNT films and optimizing the concentrations of HCNC, the hybrid film exhibits a high specific capacitance of 183.7 F g^{-1} at 10 mV s^{-1} and good cycling stability of 85% retention after 5000 cycles at 1 A g^{-1}. Our study provides potential scale-up synthesis of free-standing CNT electrode materials for high-performance supercapacitors.

1 Introduction

Flexible electronic devices have been used in a wide range of applications, such as flexible transistors, smart sensors, flexible energy harvesting and storage, touch screens, and robotic systems with skin-like sensing capabilities.[1–9] Lithium ion batteries are the current energy storage devices, but they suffer from low power densities, sluggish charge/discharge processes, and limited cycle life.[10,11] In this regard, supercapacitors are promising alternatives owing to their higher power output, faster charge/discharge rates and long cycling life.[12–15] Currently, a variety of electrode materials have been used in supercapacitors, such as RuO_2,[16] MnO_2,[17–20] polypyrrole,[21] mesoporous carbon,[22,23] and activated carbon.[24–26] However, these electrode materials are usually rigid particles. When the electrode undergoes deformation such as bending or twisting, it easily falls off the current collector, which causes the electrochemical performance to attenuate. Therefore, it is of great importance to develop flexible electrode materials without compromising electrochemical performance.

Carbon nanotubes (CNTs) have attracted extensive attention owing to its unique one-dimensional tubular structure. They have been regarded as promising electrode materials for flexible electronics due to the excellent electrical conductivity, mechanical flexibility, good chemical stability, and ready commercial availability.[27–30] Liu[31] fabricated porous CNTs through a simple approach, and the optimal sample exhibited a high specific capacitance of 331 F g^{-1} (6 M KOH, 1 A g^{-1}). In order to utilize CNTs as flexible electrodes, it is necessary to fabricate CNT macroscopic assemblies such as films. To date, several methods have been proposed for preparing CNT films, such as vacuum filtration,[32,33] solution spraying,[34] and domino-pushing.[35] However, these methods are complicated and of high cost, which are not beneficial for practical applications. We previously developed a facile method to continuously fabricate CNT films, which exhibited simultaneously excellent mechanical, electrical properties, and flexibility.[36] However, the challenge of severe aggregation between CNTs remains, which is a long-standing problem in CNT products resulting from the large surface area and strong π–π interactions or van der Waals interactions. Such aggregation will lead to the loss of active surface areas and thus degradation of the electrochemical performance.[37] In addition, the impurities (*e.g.*, Fe nanoparticles) as the commonly remaining catalysts used for CNT synthesis cannot participate in the electrochemical reactions, and reduce the specific capacitance as well as the mechanical properties. Therefore, it is necessary to prepare flexible and pure CNT films with high electrochemical performance.

In this study, we fabricate a CNT and hollow carbon nanocage (HCNC) hybrid film (CNT-HCNC) through a spray pyrolysis-based method. The HCNCs were *in situ* added into the CNT film during the continuous layer-by-layer deposition process, which is beneficial for increasing the contact areas with electrolyte. Furthermore, the residual catalyst particles in the as-prepared CNT hybrid films were effectively removed by mild cyclic voltammetry. Benefiting from the purification and enhanced transport of electrolyte, the purified CNT (PCNT)-HCNC film shows a high specific capacitance of 183.7 F g^{-1} and good cycling performance with 85% capacitance retention after 5000 cycles.

School of Mechanical and Power Engineering East China University of Science and Technology, 130 Meilong Road, Shanghai 200237, China. E-mail: jnwang@ecust.edu.cn; Tel: +86-21-64252360

† Electronic supplementary information (ESI) available. See DOI: 10.1039/d0ra09710a

2 Experimental methods

2.1 Continuous synthesis of hollow CNT assembly

The hollow cylinder-like CNT assembly was continuously synthesized at 1100–1200 °C in a horizontal furnace using a ceramic tube and nitrogen as the reactor and carrier gas, respectively. The reaction solution consisted of a liquid feedstock of ethanol with dissolved ferrocene (0.2–0.8 wt%) as the catalyst precursor and thiophene (0.05–0.3 wt%) as the growth promoter. This solution was injected into the reactor at a rate of 2–10 mL min^{-1}, which was carried into the high-temperature zone by N_2 at a flow rate of 16–32 L h^{-1}. A film in the form of cylinder formed on the inner side wall of the reactor at the downstream, and was driven out from the reactor to the air by the enclosed N_2 (Fig. 1).

2.2 Synthesis of carbon nanocage (CNC) and hollow CNC (HCNC) power

The CNC powder was prepared by a spray pyrolysis approach. C_2H_2 and N_2 gases were mixed and flowed through liquid iron carbonyl ($Fe(CO)_5$) into a quartz reactor at 700 °C. Iron carbonyl was used as the Fe precursor, N_2 as the carrier gas at a flow rate of 60 L h^{-1}, and C_2H_2 as the carbon source at 100 mL min^{-1}. Then, the carrier gas carried the as-prepared CNC powder to a large collection tank.

The CNC powder was evenly mixed with excess ammonium chloride and placed in a quartz tube. The quartz tube was pumped by a vacuum pump and then protected by nitrogen. It was then inserted into a furnace and held at 500 °C for 30 min. After heat treatment, the quartz tube was cooled to room temperature, and the sample was washed in deionized water. The final product was collected as the HCNC.

2.3 Synthesis of CNT film and CNT-HCNC film

The preparation of the CNT and CNT-HCNC films is schematically shown in Fig. 1. A winding drum with a diameter of 0.2 or 0.4 m was used for winding CNTs. It was wrapped with a paper substrate which was wetted with ethanol. As soon as the CNT cylinder was introduced on the wet paper, it shrank to a condensed and narrow CNT film. With continuous deposition on the winding drum, a pure CNT film with a controllable size was prepared. For the synthesis of a CNT-HCNC film, a methanol dispersion with different concentrations of HCNCs was used as the shrinking solution instead of ethanol. The winding rate was optimized as 4–20 m min^{-1} depending on the specific experimental conditions.

2.4 Structure characterization

The contents of CNT and Fe were evaluated by thermogravimetric analysis (TGA, Netzsch Model STA 409 PC, heating rate of 10 °C min^{-1} and a constant air flow of 20 mL min^{-1}). The structural features of CNTs and CNCs were characterized by high resolution transmission electron microscopy (HR-TEM, JEOL-2010F, accelerating voltage of 200 kV), and Raman spectroscopy (Raman, Bruker Senterra R200-L, excitation wavelength of 532 nm). The functional groups were determined by X-ray photoelectron spectroscopy (XPS, ESCALAB 250Xi). The specific surface area of the sample was calculated using the Brunauer–Emmett–Teller method (BET, TriStar 3000 V6.05 A).

2.5 Electrochemical measurements

The samples were tested using a conventional three-electrode system in a 0.5 M H_2SO_4 aqueous solution on an electrochemical workstation (CHI 760E) at room temperature. In a three-electrode system, a graphite plate and a saturated calomel electrode (SCE) were used as the counter and reference electrodes, respectively. The electrochemical impedance was measured by applying an AC voltage of 10 mV amplitude in a frequency range from 0.01 Hz to 100 kHz at an open circuit potential. To further evaluate the potential for flexible energy storage devices, a quasi-solid-state symmetric supercapacitor was constructed using two identical films as positive and negative electrodes, a cotton knitted fabric as separator and PVA/H_2SO_4 as gel electrolyte. The PVA/H_2SO_4 gel electrolyte was prepared by dissolving 5 g PVA and 5 g H_2SO_4 in 30 mL deionized water at 90 °C under vigorous stirring, followed by cooling to room temperature. The two film electrodes and cotton fabric were soaked into the gel electrolyte for 15 min and subsequently dried. Then they were assembled into a device and left for 12 h to allow electrolyte solidification. Cyclic voltammetry (CV) and galvanostatic charge–discharge were carried out in the three-electrode systems. The specific capacitance in the three-electrode system was calculated from the cyclic voltammetry (CV) measurements as follows:

$$C = \int I(V)\mathrm{d}V/2V\nu$$

where the integral term refers to the area of the CV curve, V is the potential sweep range starting from 0–1.0 V, and ν is the

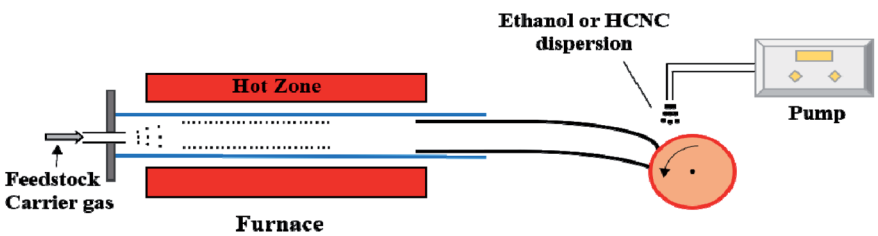

Fig. 1 Schematic diagram of the preparation process of CNT and CNT-HCNC films.

scan rate. Additionally, the galvanostatic charge and discharge (GCD) curves were used to calculate the capacitance as follows:

$$C = I\Delta t/\Delta V$$

where I, ΔV, and Δt are the discharge current, voltage range excluding the IR drop, and discharge time, respectively.

3 Results and discussion

3.1 Properties of CNT and CNT film

Fig. 2a depicts the as-obtained hollow cylinder-like CNT assembly coming out from the reactor. After having been shrunk by ethanol, a CNT film was collected on the winding drum continuously. The film could be easily curled without damage, demonstrating its excellent flexibility (Fig. 2b). The TEM images in Fig. 2c and d reveal that CNTs had a diameter of about 5–10 nm and were combined together to form a complete network structure. The Fe nanoparticles produced from ferrocene were coated with carbon layers (Fig. 2d). Their content was determined as 31.7 wt% by TG analysis (Fig. 2e, the 45.35 wt% residue was assumed to be Fe_2O_3). The I_G/I_D ratio was determined to be 3.38 in the Raman spectra (Fig. 2f), suggesting the high quality and high degree of graphitization of the as-prepared CNT film.

3.2 Electrochemical performance of PCNT film

The electrochemically inactive Fe nanoparticles inevitably contributes to a substantial portion of the electrode weight which will reduce the specific capacitance of the device.[38] Therefore, it is necessary to gently remove them without damaging the CNT structure. We infiltrated a 0.5 M sulfuric acid electrolyte solution into the CNT film, and performed 20 cycles from −0.4 V to 1.6 V at a scanning rate of 50 mV s^{-1} as done in a previous study.[39] As shown in Fig. 3a, a sharp peak located at 0.1–0.3 V was observed initially, evidencing the presence of Fe nanoparticles in the CNT film. During the 15 cycles, the intensity of the peak gradually reduced, and nearly disappeared at the 20th cycle (Fig. S1b†), indicating that the Fe particles in the film had been largely dissolved. Compared with the pristine

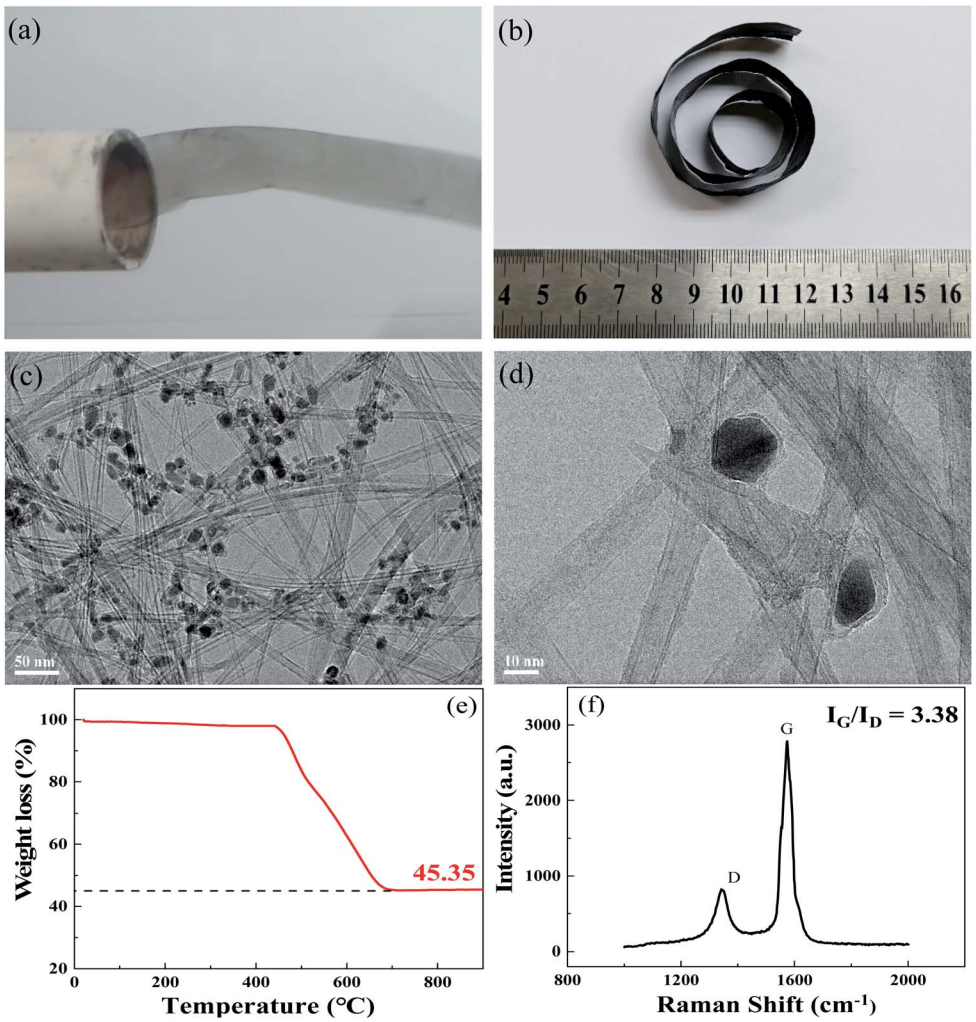

Fig. 2 (a) Hollow cylinder assembled from CNTs. (b) Flexible and winded CNT film. (c) TEM image of the CNTs in the cylinder. (d) HRTEM image of CNTs. (e) TG curve of CNT film. (f) Raman spectrum of CNT film.

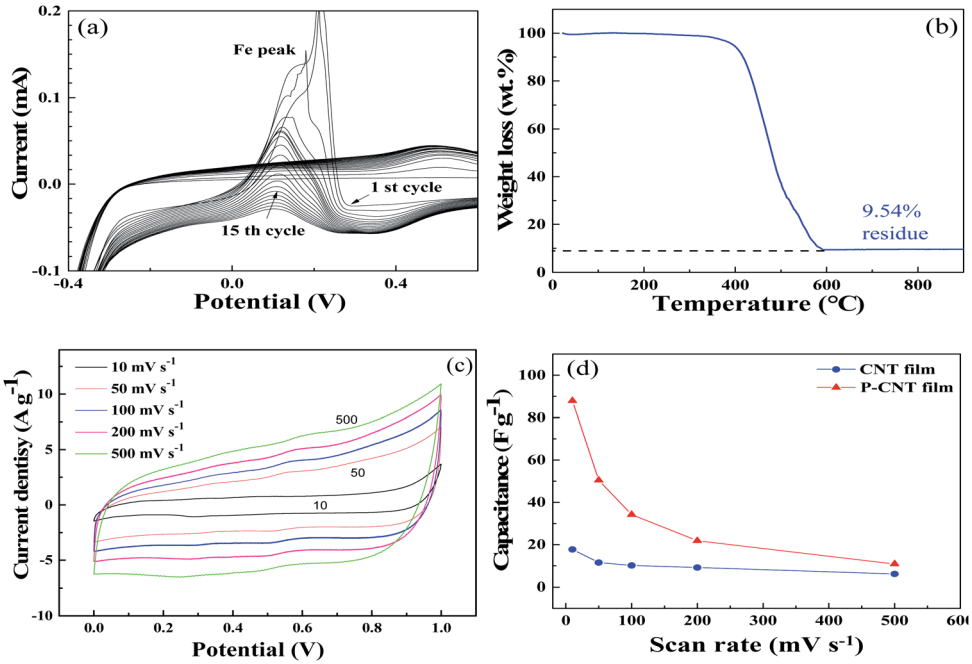

Fig. 3 (a) CV curves during the purification process. (b) TG curve of PCNT. (c) CV curves of PCNT. (d) Specific capacitances of the original CNT and PCNT films at various scanning rates.

CNT (Fig. 2c), the TEM image of the purified CNT (Fig. S2†) further confirmed the removal of catalyst particles in the CNT. TGA was used to determine the remaining content of Fe in the CNT film after electrochemical purification. As shown in Fig. 3b, the content of residual Fe was reduced to 6.7 wt%, indicating the effectiveness of this purification method.

The specific capacitance of the original CNT film and PCNT film were determined by CV measurements, as shown in Fig. S1a,† 3c and d respectively. Compared to the pristine CNT film, the specific capacitance of the purified CNT (PCNT) film was significantly improved. When the scanning rate was 10 mV s^{-1}, the specific capacitance of the PCNT film reached 87.8 F g^{-1}, about 5 times that of the original CNT film, indicating that purification had an effective activation effect on the electrochemical performance of CNT films. The increased specific capacitance can be mainly ascribed to the removal of impurities, which can not only reduce the absolute mass of electrodes but also create new opened microscopic pores during the purification process. However, when the scanning rate reached 500 mV s^{-1}, the specific capacitances of the original CNT and PCNT film were not significantly different, indicating that the compact stacking and aggregation of CNTs limited the entry and transportation of the electrolyte.

3.3 Electrochemical performance of PCNT-HCNC film

To solve the problem of CNT stacking, HCNCs were successfully prepared and added within the CNT film. Initially, the CNC particles were prepared with Fe nanoparticles encapsulated (Fig. S3a and b†). With further heat treatment in the presence of ammonium chloride, the Fe nanoparticles within the CNCs were effectively removed without damage to the structure of CNCs, giving rise to HCNCs with a diameter of 2–5 nm (Fig. S3c and d†). The hybrid films with different weight ratios of PCNTs and HCNCs were prepared, as shown in Fig. S4.† It was found that with the increased amount of HCNC, the specific capacitance of the film became larger (Fig. S5a and b†). However, when the concentration of HCNC was too high, the specific capacitance decreased (Fig. S5c†). The concentration of HCNC in the methanol was 1.0 mg mL^{-1}, and the PCNT-HCNC film (denoted as PCNT-HCNC-1.0) showed the best performance. Fig. 4a shows the CV curves of the film at different scan rates ranging from 10 to 500 mV s^{-1}. The curves retained almost a rectangular shape from 0 to 1 V over a wide range of scan rates (Fig. S5d†), suggesting the electrochemical double layer capacitor nature in the charge–discharge process, which might result from the fast diffusion process of electrolyte ions into/out of the electrode material. The XPS (Fig. S6†) demonstrated that oxygen existed in the sample with a low atomic ratio of 6.2%. The oxygen atoms were mainly in the form of C–O and a small fraction of C=O, which could also contribute to the electrochemical performance through a redox reaction. As shown in Fig. 4b, the PCNT-HCNC-1.0 exhibits a high specific capacitance of 183.7 F g^{-1} at 10 mV s^{-1}, which is twice as large as that of the PCNT film, indicating that the addition of HCNC nanoparticles significantly increased the electrochemical surface area of the film. When the scanning rate was increased to 500 mV s^{-1}, the specific capacitance of PCNT-HCNC-1.0 was 13 times that of the PCNT film, which indicates that the HCNC can effectively improve the rate capability.

We used a schematic diagram to describe the role of HCNC in the film (Fig. 4c). For the original CNT film, the CNTs densely stacked with each other due to the strong van der Waals force.

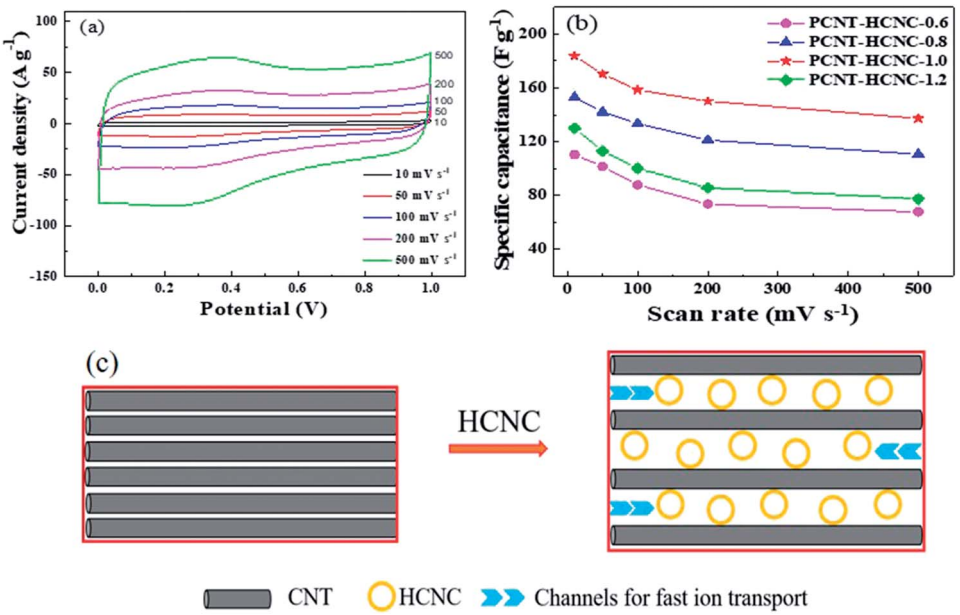

Fig. 4 (a) CV curves of the PCNT-HCNC-1.0 film at different scan rates. (b) Specific capacitance curves of different PCNT-HCNC films. (c) Schematic diagram of the role of hollow carbon nanocages.

In addition, the hydrophobic nature of the CNT led to the difficulty of the conductive ion transport in the film, especially at high scanning rates. As a comparison, the addition of HCNC nanoparticles could effectively loosen the densely packed CNTs and provide channels for the electrolyte ions. However, when the amount of HCNC was further increased, the alignment of CNTs in the film would be reduced, leading to the increased thickness of the film and thus reduced utilization of the active materials.

To probe into the electrochemical improvement of the PCNT-HCNC hybrid films, the electrochemical impendence spectra (EIS) were measured (Fig. 5) with an AC voltage amplitude of 10 mV in the frequency range from 0.01 Hz to 100 kHz. In the low frequency region, all of the samples showed an inclination at an angle of 75°, indicating their capacitive behaviour. In the high frequency region, the semicircles were often associated with the charge transfer resistance (R_{ct}) representing the ion transfer efficiency at electrolyte/electrode interface. With the increase of HCNC in the composite, the R_{ct} values were 11.21 Ω for PCNT-HCNC-0.6, 7.58 Ω for PCNT-HCNC-0.8, 5.72 Ω for PCNT-HCNC-1.0, and 10.43 Ω for PCNT-HCNC-1.2. It was found that the PCNT-HCNC-1.0 showed the lowest R_{ct} among all the samples, indicative of their fast reaction kinetics due to the sufficient channels for ions and thus significantly enhanced electrochemical properties.

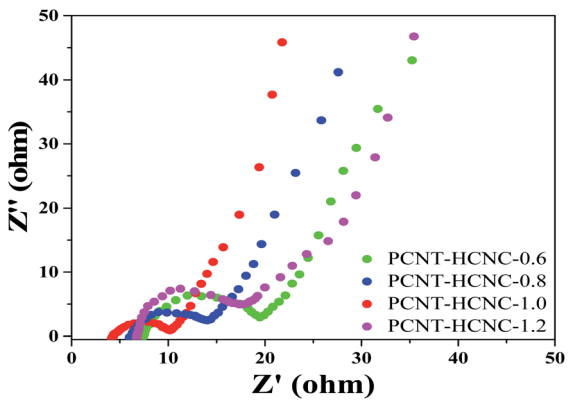

Fig. 5 Nyquist plots for the different PCNT-HCNC hybrid film-based EDL supercapacitors.

GCD measurements were carried out at different current densities to evaluate the electrochemical performance of the electrode materials. The GCD curves of PCNT-HCNC-1.0 at different current densities are shown in Fig. 6a. A minimal IR drop was observed, suggesting the low internal resistance and the fast ion diffusion. A high specific capacitance of 161 F g^{-1} was achieved for PCNT-HCNC-1.0 at 1 A g^{-1}, which decreased to 145 F g^{-1} at 2 A g^{-1} and 125 F g^{-1} at 5 A g^{-1} (Fig. 6b). It should be noted that a specific capacitance of 113 F g^{-1} can still be achieved at 10 A g^{-1} with a retention of 70%, suggesting its excellent rate capability.[40–42]

To demonstrate its potential application in flexible devices, we fabricated an all-solid-state symmetric supercapacitor based on the PCNT-HCNC-1.0 electrodes. The capacitor exhibited an excellent electrochemical stability with a retention of above 85% after 5000 cycles at 1 A g^{-1} (Fig. 6c). LED light could be easily lit up as shown in Fig. 6d. In addition, when the supercapacitor was bent to different angles (0, 30, 90, and 180°) as shown in Fig. S7a†, the specific capacitance showed negligible variation. Even after bending for 1000 times, there was no significant reduction in capacitance (Fig. S7b†), further revealing the excellent flexibility of the capacitor. Compared with the commercial activated carbons and other carbon-based supercapacitors, the PCNT-HCNC-1.0 had higher energy storage

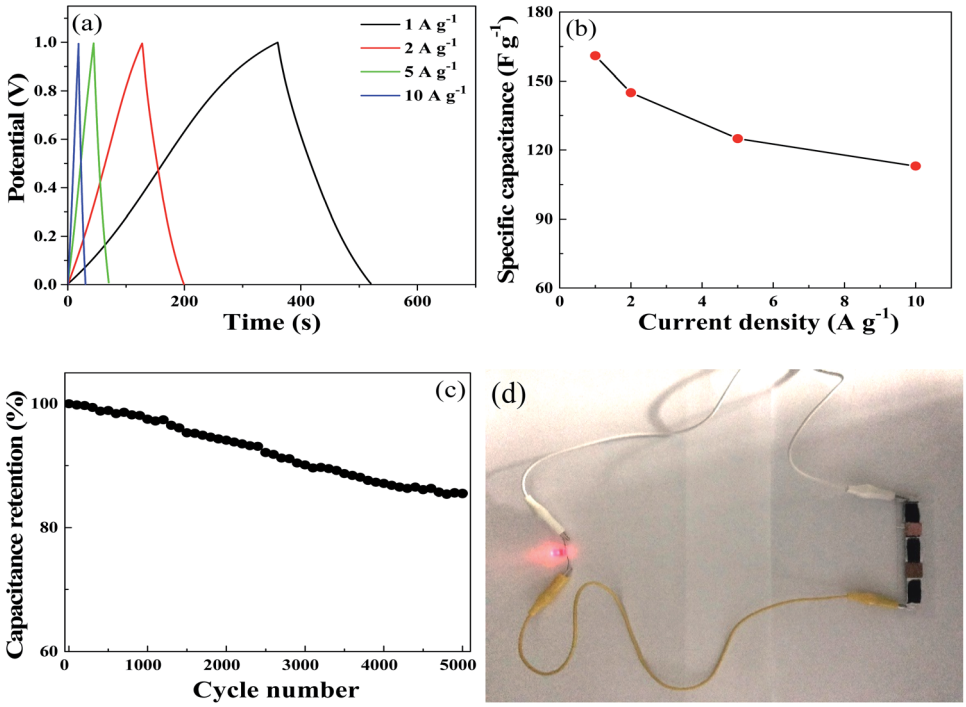

Fig. 6 (a) GCD curves of the PCNT-HCNC film at different current densities. (b) Specific capacitance of PCNT-HCNC at various current densities. (c) Cycle life of CNT-HCNC measured at a current density of 1 A g^{-1}. (d) Digital image of a LED light lit by the PCNT-HCNC film.

performance in terms of the areal capacitance and volumetric energy density (Tables S1, S2 and Fig. S8†).

4 Conclusions

In summary, we prepared a CNT/CNC film through a facile layer-by-layer strategy. Through a mild CV cycling process, most of the residual Fe particles in the film can be removed, thus increasing the specific capacitance of the film. In addition, the purification process can also create new opened microscopic pores during the removal of Fe nanoparticles, improving the electrochemical activity area and the specific capacitance of the film. The *in situ* addition of HCNCs in the film is beneficial for preventing the CNT stacking and thus promoting the electrolyte transport. As a result, the PCNT-HCNC film can achieve a high specific capacitance of 183.7 F g^{-1} at 10 mV s^{-1}, good cycling performance with 85% capacitance retention after 5000 cycles, and excellent flexibility. Our study provides a potential strategy toward the preparation of high-performance CNT-based electrode materials for flexible supercapacitors.

Conflicts of interest

There are no conflicts to declare.

Acknowledgements

This research was supported by National Key R&D Program of China (2018YFA0208404), National Natural Science Foundation of China (U1362104), and Innovation Program of Shanghai Municipal Education Commission.

References

1 M.-L. Hammock, A. Chortos, B.-C. Tee, J.-B. Tok and Z. Bao, *Adv. Mater.*, 2013, **25**, 5997–6038.
2 Y.-S. Rim, S.-H. Bae, H. Chen, D.-M. Nicholas and Y. Yang, *Adv. Mater.*, 2016, **28**, 4415–4440.
3 M. Lim, D. H. Kim, C. Park, Y. Lee, S. Han, Z. Li, R. Williams and I. Park, *ACS Nano*, 2012, **6**, 598–608.
4 K. Takei, T. Takahashi, J.-C. Ho, H. Ko, A.-G. Gillies, P.-W. Leu, R.-S. Fearing and A. Javey, *Nat. Mater.*, 2010, **9**, 821–826.
5 Y. Li, R. Yao, H. Wang, X. Wu, J. Wu, X. Wu and W. Qin, *ACS Appl. Mater. Interfaces*, 2017, **9**, 11711–11720.
6 S. Xu, Y. Qin, C. Xu, Y. Wei, R. Yang and Z. L. Wang, *Nat. Nanotechnol.*, 2010, **5**, 366–373.
7 P. Barquinha, S. Pereira, L. Pereira, P. Wojcik, P. Grey, R. Martins and E. Fortunato, *Adv. Electron. Mater.*, 2015, **1**, 1500030/1–1500030/7.
8 G. Fiori, F. Bonaccorso, G. Iannaccone, T. Palacios, D. Neumaier, A. Seabaugh, S. Banerjee and L. Colombo, *Nat. Nanotechnol.*, 2014, **9**, 768–779.
9 Q. Cao, H. Kim, N. Pimparkar, J.-P. Kulkarni, C. Wang, M. Shim, K. Roy, M.-A. Alam and J.-A. Rogers, *Nature*, 2008, **454**, 495–500.
10 M. Beidaghi and Y. Gogotsi, *Energy Environ. Sci.*, 2014, **7**, 867–884.

11 D. Yu, Q. Qian, L. Wei, W. Jiang, K. Goh, J. Wei, J. Zhang and Y. Chen, *Chem. Soc. Rev.*, 2015, **44**, 647–662.
12 W. Gao, N. Singh, L. Song, Z. Liu, A. L. M. Reddy, L. Ci, R. Vajtai, Q. Zhang, B. Wei and P. M. Ajayan, *Nat. Nanotechnol.*, 2011, **6**, 496–500.
13 P. Huang, C. Lethien, S. Pinaud, K. Brousse, R. Laloo, V. Turq, M. Respaud, A. Demortière, B. Daffos, P. L. Taberna, B. Chaudret, Y. Gogotsi and P. Simon, *Science*, 2016, **351**, 691–695.
14 G. Wang, L. Zhang and J. Zhang, *Chem. Soc. Rev.*, 2012, **41**, 797–828.
15 Z. Yu, L. Tetard, L. Zhai and J. Thomas, *Energy Environ. Sci.*, 2015, **8**, 702–730.
16 Z.-S. Wu, D.-W. Wang, W. Ren, J. Zhao, G. Zhou, F. Li and H.-M. Cheng, *Adv. Funct. Mater.*, 2010, **20**, 3595–3602.
17 W. Chen, Y. He, X. Li, J. Zhou, Z. Zhang, C. Zhao, C. Gong, S. Li, X. Pan and E. Xie, *Nanoscale*, 2013, **5**, 11733–11741.
18 C. Xiong, T. Li, A. Dang, T. Zhao, H. Li and H. Lv, *J. Power Sources*, 2016, **306**, 602–610.
19 W. Ma, S. Chen, S. Yang, W. Chen, Y. Cheng, Y. Guo, S. Peng, S. Ramakrishna and M. Zhu, *J. Power Sources*, 2016, **306**, 481–488.
20 S. He and W. Chen, *J. Power Sources*, 2015, **294**, 150–158.
21 J. Jyothibasu and R.-H. Lee, *J. Mater. Chem. A*, 2020, **8**, 3186–3202.
22 R. Liu, L. Wan, S. Liu, L. Pan, D. Wu and D. Zhao, *Adv. Funct. Mater.*, 2015, **25**, 526–533.
23 X. Zhang, Q. Lin, X. Zhang and K. Peng, *J. Power Sources*, 2018, **401**, 278–286.
24 K. Wang, N. Zhao, S. Lei, R. Yan, X. Tian, J. Wang, Y. Song, D. Xu, Q. Guo and L. Liu, *Electrochim. Acta*, 2015, **166**, 1–11.
25 L. Yu, L. Hu, B. Anasori, Y. Liu, Q. Zhu, P. Zhang, Y. Gogotsi and B. Xu, *ACS Energy Lett.*, 2018, **3**, 1597–1603.
26 J.-H. Lee, H. Kim, E. Baek, M. Pecht, S. Lee and Y. Lee, *J. Power Sources*, 2016, **301**, 348–354.
27 Z. Cao and B. Wei, *Energy Environ. Sci.*, 2013, **6**, 3183–3201.
28 S. Gao, K. Wang, Z. Du, Y. Wang, A. Yuan, W. Lu and L. Chen, *Carbon*, 2015, **92**, 254–261.
29 N. Rouhi, D. Jain and P.-J. Burke, *ACS Nano*, 2011, **5**, 8471–8487.
30 Q. Cao and J.-A. Rogers, *Adv. Mater.*, 2009, **21**, 29–53.
31 W. Liu, Y. Tang, Z. Sun, S. Gao, J. Ma and L. Liu, *Carbon*, 2017, **115**, 754–762.
32 J. Han, H. Zhang, M. Chen, D. Wang, Q. Liu, Q. Wu and Z. Zhang, *Carbon*, 2015, **94**, 101–113.
33 J. Han, H. Zhang, P. Chu, A. Imani and Z. Zhang, *Compos. Sci. Technol.*, 2015, **114**, 1–10.
34 Q. Liu, T. Fujigaya, H. M. Cheng and N. Nakashima, *J. Am. Chem. Soc.*, 2010, **132**, 16581–16586.
35 D. Wang, P. Song, C. Liu, W. Wu and S. Fan, *Nanotechnology*, 2008, **19**, 075609.
36 W. Xu, Y. Chen, H. Zhan and J. Wang, *Nano Lett.*, 2016, **16**, 946–952.
37 M.-Q. Zhao, Q. Zhang, J.-Q. Huang, G.-L. Tian, J.-Q. Nie, H. J. Peng and F. Wei, *Nat. Commun.*, 2014, **5**, 3410.
38 Y. Wang, Z. Wang, X. Yu, B. Li, F. Kang and Y.-B. He, *J. Mater. Res.*, 2018, **33**, 1058–1073.
39 X.-X. Huang, Y. Chen, X.-X. Wang and J.-N. Wang, *J. Mater. Chem. A*, 2015, **3**, 7862–7869.
40 P. Xu, T. Gu, Z. Cao, B. Wei, J. Yu, F. Li, J. H. Byun, W. Lu, Q. Li and T. W. Chou, *Adv. Energy Mater.*, 2014, **4**, 1300759.
41 X. Han, M.-R. Funk, F. Shen, Y.-C. Chen, Y.-Y. Li, C. Campbell, J. Dai, X. Yang, J.-W. Kim, Y.-L. Liao, J. Connell, V. Barone, Z. Chen, Y. Lin and L. B. Hu, *ACS Nano*, 2014, **8**, 8255–8265.
42 T. Wang, L.-X. Wang, D.-L. Wu, W. Xia and D.-Z. Jia, *Sci. Rep.*, 2015, **5**, 09591.